UC Berkeley
UC Berkeley Previously Published Works

Title

Optically induced changes in the band structure of the Weyl charge-density-wave compound (TaSe4)2I

Permalink

Journal

ISSN

Authors

Crepaldi, A
Puppin, M
Gosálbez-Martínez, D
et al.

Publication Date

DOI

Copyright Information

Peer reviewed

PAPER • OPEN ACCESS

Optically induced changes in the band structure of the Weyl charge-density-wave compound $(TaSe_4)_2I$

View the article online for updates and enhancements.

Journal of Physics: Materials

PAPER

Optically induced changes in the band structure of the Weyl charge-density-wave compound $(TaSe_4)_2I$

A Crepaldi[1,2,3,*] ⓘ, M Puppin[3,4] ⓘ, D Gosálbez-Martínez[2,5], L Moreschini[6,7] ⓘ, F Cilento[8], H Berger[2],
O V Yazyev[2,5] ⓘ, M Chergui[3,4] and M Grioni[2,3]

1   Dipartimento di Fisica, Politecnico di Milano, Piazza Leonardo da Vinci 32, 20133 Milan, Italy
2   Institute of Physics, École Polytechnique Fédérale de Lausanne (EPFL), CH-1015 Lausanne, Switzerland
3   Lausanne Centre for Ultrafast Science (LACUS), École Polytechnique Fédérale de Lausanne (EPFL), CH-1015 Lausanne, Switzerland
4   Laboratory of Ultrafast Spectroscopy, ISIC, École Polytechnique Fédérale de Lausanne (EPFL), CH-1015 Lausanne, Switzerland
5   National Centre for Computational Design and Discovery of Novel Materials MARVEL, École Polytechnique Fédérale de Lausanne
    (EPFL), CH-1015 Lausanne, Switzerland
6   Materials Sciences Division, Lawrence Berkeley National Laboratory, Berkeley, CA 94720, United States of America
7   Department of Physics, University of California, Berkeley, CA 94720, United States of America
8   Elettra—Sincrotrone Trieste S.C.p.a., Strada Statale 14 - km 163.5 in AREA Science Park, 34149 Basovizza, Trieste, Italy
*   Author to whom any correspondence should be addressed.

E-mail: alberto.crepaldi@polimi.it

Abstract

Collective modes are responsible for the emergence of novel quantum phases in topological materials. In the quasi-one dimensional (1D) Weyl semimetal $(TaSe_4)_2I$, a charge density wave (CDW) opens band gaps at the Weyl points, thus turning the system into an axionic insulator. Melting the CDW would restore the Weyl phase, but 1D fluctuations extend the gapped regime far above the 3D transition temperature ($T_{CDW} = 263$ K), thus preventing the investigation of this topological phase transition with conventional spectroscopic methods.

    Here we use a non-equilibrium approach: we perturb the CDW phase by photoexcitation, and we monitor the dynamical evolution of the band structure by time- and angle-resolved photoelectron spectroscopy. We find that, upon optical excitation, electrons populate the linearly dispersing states at the Fermi level (E_F), and fill the CDW gap. The dynamics of both the charge carrier population and the band gap renormalization (BGR) show a fast component with a characteristic time scale of a few hundreds femtoseconds. However, the BGR also exhibits a second slow component on the μs time scale. The combination of an ultrafast response and of persistent changes in the spectral weight at E_F, and the resulting sensitivity of the linearly dispersing states to optical excitations, may explain the high performances of $(TaSe_4)_2I$ as a material for broadband infrared photodetectors.

1. Introduction

The Weyl topological phase, initially put forward in magnetic pyrochlore iridates [1], and later observed in non-centrosymmetric TaAs [2], emerges in materials with strong spin–orbit coupling (SOC), in the absence of spin degeneracy [3, 4]. Weyl fermions appear as pairs of crossing points induced by band inversion, each one carrying opposite topological charges [3]. They behave like magnetic monopoles in momentum space, and are at the origin of unique electromagnetic responses, such as the chiral magnetic anomaly [5]. In a Weyl semimetal the coupling to the electromagnetic field contains a term that mimics an axion field [6]. Axions, which were originally introduced in high-energy particle physics [7] and might explain dark matter [8], emerge in gapped phases of topological materials [9] and lead to exotic phenomena such as the fractional quantum Hall effect [10]. Many-body interactions and a reduced dimensionality can induce the formation of a charge density wave (CDW) state [11], and open gaps at the Weyl points. The sliding modes of the

CDW—phasons—are proposed to behave like axions, thereby realizing a so-called 'axionic insulator' [1]. Recently, this mechanism was proposed to explain the magnetotransport properties of $(TaSe_4)_2I$, characterized by a quadratic longitudinal magnetoconductance, and by a $\cos^2$ dependence on the angle between current and magnetic field [12]. This finding sparked new interest in $(TaSe_4)_2I$, with special emphasis on its topological nature [13], and on the formation of the axionic insulator phase [14].

$(TaSe_4)_2I$ is a quasi-one-dimensional (1D) compound with infinite Ta chains, whose electronic and transport properties are renormalized by collective modes [15]. The formation of a CDW state, accompanied by a lattice distortion at $T_{CDW} = 263\,K$ [16] appears as an anomaly in the electronic transport [17]. The complex distortion arises from the mixing between an electronic-coupled optical phonon mode, associated with a Ta-tetramerization [18], and a long-wavelength acoustic shear mode [19]. It differs from the Ta-tetramerization expected in a purely ionic model for a 1/4-filled band [20, 21]. The CDW is incommensurate, and multiple periodicities are observed by angle-resolved photoelectron spectroscopy (ARPES) in the momentum distribution of the spectral weight [22]. The contribution of the chain tetramerization to the opening of the CDW band gap has been recently assessed by density functional theory (DFT) calculations [23]. In the weak electron–phonon coupling limit, the incommensurability results from the interchain interaction and the Peierls-like instability is driven by nesting large portions of the distorted 1D open Fermi surface [24]. On the other hand, a strong reduction of spectral weight near the Fermi level E_F, even at temperatures above T_{CDW}, indicates that electron–phonon coupling is strong in $(TaSe_4)_2I$. Indeed, puzzling transport properties and a semiconductor-like behavior both above and below T_{CDW} [24] are consistent with the formation of small polarons [25]. Strong electron–phonon coupling is also suggested by a recent scanning tunneling microscopy and spectroscopy study to explain the bias-independent CDW modulation amplitude [26].

Although the emergence of axions in $(TaSe_4)_2I$ is supported by its electrodynamical response, the associated spectroscopic signatures still await confirmation. Fermi arcs spanning the entire Brillouin zone (BZ) are calculated for the (001) surface, which is orthogonal to the chain direction and not accessible to ARPES. Several surface states form arcs dispersing next to the bulk bands in the (110) cleavage planes [13], but resolving these surface states is a challenging task for ARPES owing to the broad polaronic line shapes [25]. Interesting information could be retrieved by inspecting the spectroscopic changes across the topological phase transition from the low-temperature axionic insulator to the high-temperature Weyl phase. However, in 1D materials the CDW band gap fully closes only well above T_{CDW} due to strong 1D fluctuations [27, 28], and this hinders the study of the transition with conventional spectroscopic methods.

In this article we explore the possibility to use an intense optical excitation to perturb and melt the CDW state, thus restoring the Weyl phase by the dynamical closure and filling of the CDW band gap. We have employed time-resolved ARPES (trARPES), which can track changes in the band structure of CDW materials [29–32]. We find that, upon optical excitation, electrons populate the linearly dispersing states around E_F. We also find that the whole valence band (VB) moves towards smaller binding energies. We attribute this energy shift to a change in screening following the renormalization of the CDW band gap. Spectral changes occur on two greatly different temporal regimes: we observe an ultrafast component on the sub-ps time scale, and a shift persisting up to the μs time scale, signaling an increased lattice temperature. The optically induced increase of the spectral weight at E_F could explain the high performances of $(TaSe_4)_2I$ as a material for broadband near-infrared photodetectors [33].

2. Methods

2.1. Experiment

$(TaSe_4)_2I$ single crystals were synthetized via chemical vapor transport method starting from a stoichiometric mixture of high purity elements, sealed in a quartz crucible with a temperature gradient between $480\,°C$ and $510\,°C$ [34]. Metallic posts were glued on the surface of needle-like crystals, with typical sizes $5 \times 0.5 \times 0.2\,mm^2$. Successively, the crystals were post-cleaved at room temperature at a base pressure better than 2×10^{-10} mbar. ARPES experiments were performed at $T = 120\,K$ at beam line 7.0.2 of the Advanced Light Source (Berkeley), at a photon energy of 95 eV, with energy and momentum resolution equal to 30 meV and $0.01\,Å^{-1}$. We performed the trARPES measurements at the LACUS facility of the EPFL [35]. The pump was the s-polarized fundamental of a Ti-sapphire laser centered at ~ 1.6 eV (780 nm). The probe was s-polarized, with an energy of 27 eV, corresponding to the 17th harmonic generated in argon. The fluence impinging on the sample was varied between $0.1\,mJ\,cm^{-2}$ and $0.55\,mJ\,cm^{-2}$. We collected data at room temperature and at 80 K, with a combined temporal, energy and momentum resolution equal to 60 fs, 200 meV and $0.007\,Å^{-1}$.

2.2. Theory

Band structure calculations were performed within the DFT using the plane-wave pseudopotential method as implemented in the Quantum-Espresso package [36, 37]. We used the Perdew–Burke–Ernzerhof [38] exchange-correlation functional and included SOC using the fully relativistic ultrasoft pseudopotentials from the PSlibrary [39]. We employed a 60 Ry plane-wave kinetic energy cutoff, a 0.01 Ry smearing and an $8 \times 8 \times 8$ Monkhorst–Pack grid.
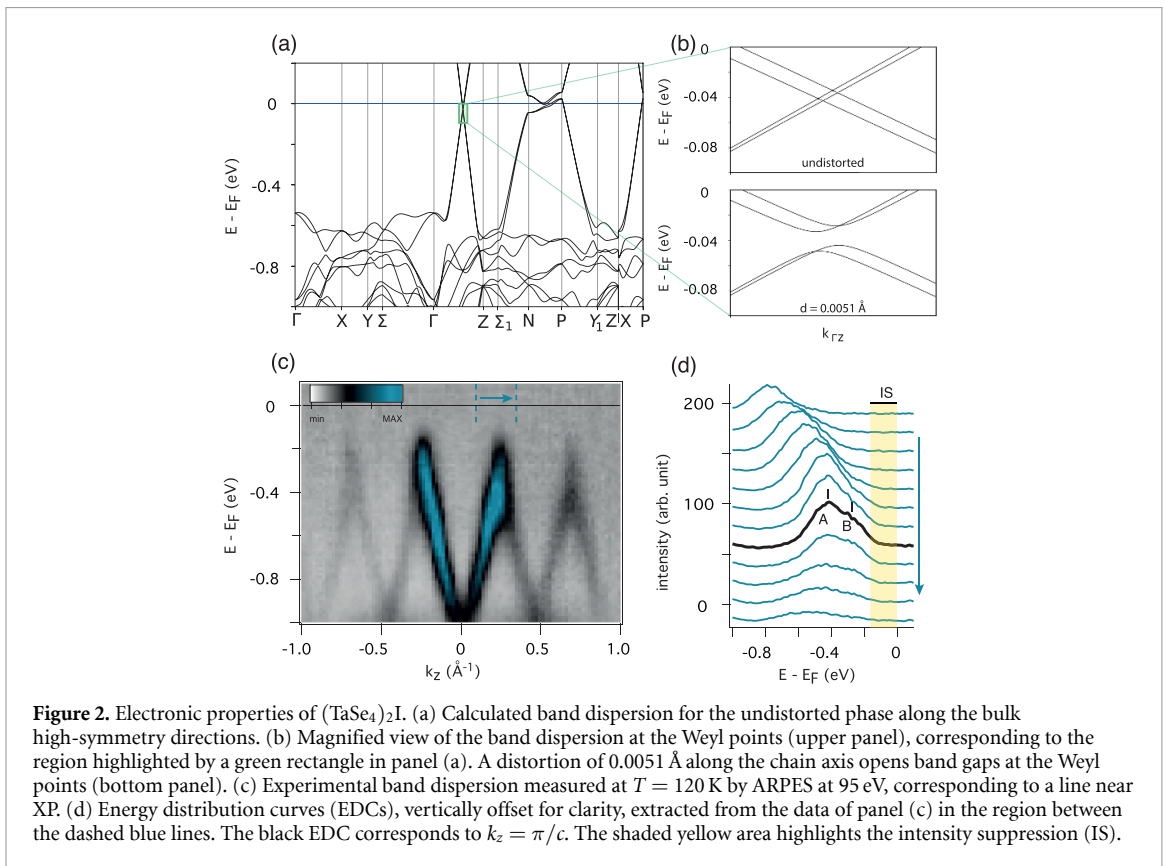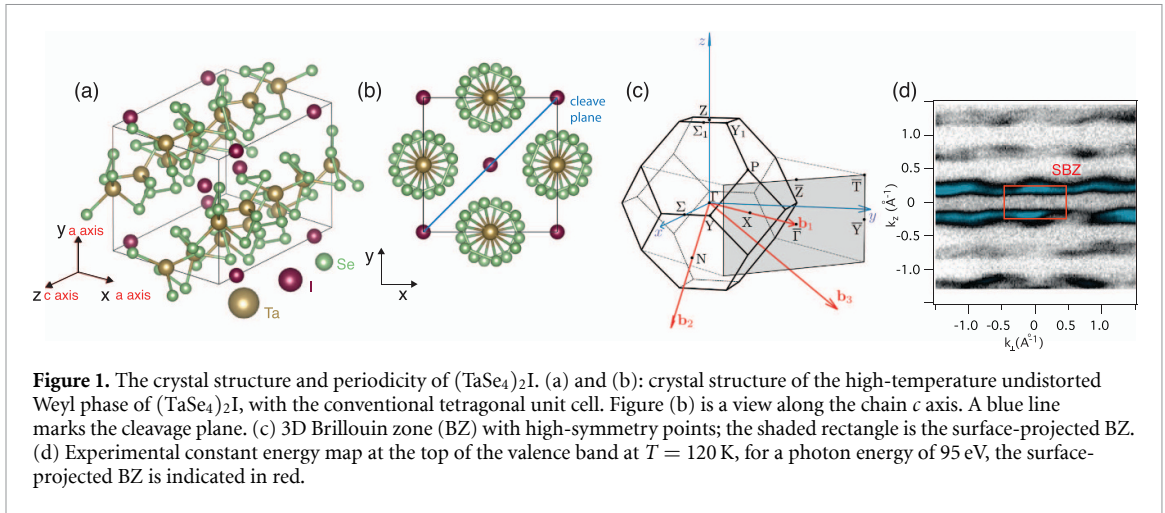
3. Results and discussion

3.1. Crystal and electronic structure of $(TaSe_4)_2I$

Figures 1(a) and (b) show the crystal structure of $(TaSe_4)_2I$ in the undistorted Weyl phase, and the conventional tetragonal unit cell, with $a = b = 9.531$ Å and $c = 12.824$ Å. Panel (a) is a tilted view, while (b) is a view along the c axis, parallel to the $(TaSe_4)$ chains and to the z axis. Along the chain the four Ta atoms are surrounded by Se_4 rectangles rotated by 45°. As a result, the isolated $(TaSe_4)_4$ chain is a chiral helix with an eightfold *non-crystallographic* screw axis [13]. Shi *et al* discussed how the electronic and topological properties of the isolated screw-symmetric chain evolve into those of the bulk crystal by considering the weak coupling between the two chains within the unit cell [13]. $(TaSe_4)_2I$ belongs to space group 97 (I422), which is symmorphic and chiral and therefore allows for the emergence of exotic fermions such as Kramers–Weyl fermions [40], whose existence was recently confirmed in Te [41]. The body-centered tetragonal unit cell has half the volume of the conventional cell, with primitive lattice vectors: $\mathbf{a}_1 = (-a/2, a/2, c/2)$, $\mathbf{a}_2 = (a/2, a/2, c/2)$, and $\mathbf{a}_3 = (a/2, a/2, -c/2)$. Figure 1(c) shows the 3D BZ, where $\Gamma Z = 0.49$ Å^{-1}, $\Gamma X = 0.466$ Å^{-1} and $XP = 0.245$ Å^{-1} [24]. Cleavage naturally occurs at the iodine (110) planes, indicated by a blue line in figure 1(b). In figure 1(c) the shaded rectangle indicates the surface-projected BZ. The ARPES constant energy map of figure 1(d), measured with a photon energy of 95 eV at the top of the VB, reveals ondulating open contours in the direction orthogonal to the chains, consistent with the quasi-1D nature of the underlying states. The periodicity of the contour matches the one expected for the (110) surface termination, in agreement with previous studies [13, 24, 26, 42]. Our data cannot resolve the presence of surface states and Fermi arcs predicted by theory [13], whose signal could be enhanced or suppressed by proper surface preparation, as similarly reported in other Weyl semimetals [43, 44]. Heat-treating $(TaSe_4)_2I$ has already proved to be a viable tool to modify the band structure by partial loss of the iodine atoms at the surface [42].

Figure 2(a) shows the calculated band structure in the high-temperature Weyl phase. Our results reproduce previous findings, in particular the presence of quasi-1D states linearly dispersing along the ΓZ direction and crossing E_F near $k_z = \pi/c$ [20, 24], reminiscent of the symmetry-enforced crossing of the isolated chain [13]. Figure 2(b) shows a magnified view of the region around the Weyl points, highlighted by the green rectangle in figure 2(a). We compare the band dispersion in the undistorted structure (upper panel) and after a distortion of 0.0051 Å in the chain direction, corresponding to the long-long-short-short Ta-tetramerization analyzed in detailed by Zhang *et al* [23]. Additional calculations reveals that even a smaller distortion is sufficient to open a band gap annihilating the Weyl points. The effect of the distortion farther away from E_F is negligible. On the other hand, we checked that positive and negative compressions, which do not affect the crystal symmetry, leave the Weyl points unchanged.

Figure 2(c) displays the experimental band dispersion, acquired in the CDW phase at 120 K with a photon energy of 95 eV. According to the literature, at this photon energy ARPES probes the electronic states along a line in the 3D BZ close to XP between the 5th and the 6th BZs [24]. This photon energy is a good reference for the trARPES data which, for a photon energy of 27 eV, also sample a line close to XP, between the 3rd and the 4th BZs. We use the high-resolution synchrotron data to illustrate the preeminent characteristics of the band dispersion. The spectral weight is distributed mostly in one single branch of the Weyl cone. This asymmetry is not caused by measurement geometry/alignment issues as it is reported in all ARPES studies with variable photon energies in the (21–88) eV range [13, 22, 24, 25, 42]. This effect well exemplifies how the spectral weight distribution is controlled by the strength of the periodic potential, and it can even reflect the presence of competing periodicities [22]. The opening of the CDW band gap is better shown by the energy distribution curves (EDCs) of figure 2(d), extracted from panel (c) between the dashed lines. The EDCs reveal overlapping contributions labeled A and B, well visible near $k_z = \pi/c$ (black line). In previous ARPES studies they were alternatively attributed to two VB components [25], or to distinct VB and conduction band (CB) features [13, 24]. In both scenarios the data reflect a polaronic line shape in the strong coupling limit, where the measured peak belongs to the incoherent part of the spectral function corresponding to the envelope of the phonon-excited satellites. The incoherent part of the spectral function is shifted to higher binding energies with respect to the zero-phonon coherent quasiparticle (QP), whose spectral weight is exponentially suppressed [25]. The measured intensity suppression (IS) induced by the

Figure 1. The crystal structure and periodicity of $(TaSe_4)_2I$. (a) and (b): crystal structure of the high-temperature undistorted Weyl phase of $(TaSe_4)_2I$, with the conventional tetragonal unit cell. Figure (b) is a view along the chain *c* axis. A blue line marks the cleavage plane. (c) 3D Brillouin zone (BZ) with high-symmetry points; the shaded rectangle is the surface-projected BZ. (d) Experimental constant energy map at the top of the valence band at $T = 120$ K, for a photon energy of 95 eV, the surface-projected BZ is indicated in red.

Figure 2. Electronic properties of $(TaSe_4)_2I$. (a) Calculated band dispersion for the undistorted phase along the bulk high-symmetry directions. (b) Magnified view of the band dispersion at the Weyl points (upper panel), corresponding to the region highlighted by a green rectangle in panel (a). A distortion of 0.0051 Å along the chain axis opens band gaps at the Weyl points (bottom panel). (c) Experimental band dispersion measured at $T = 120$ K by ARPES at 95 eV, corresponding to a line near XP. (d) Energy distribution curves (EDCs), vertically offset for clarity, extracted from the data of panel (c) in the region between the dashed blue lines. The black EDC corresponds to $k_z = \pi/c$. The shaded yellow area highlights the intensity suppression (IS).

strong electron–phonon coupling and the CDW is highlighted by a shaded yellow area. The opening of the CDW (pseudo)gap and the IS were already observed in previous ARPES experiments [13, 24]. The latter study shows that the spectral features persist up to room temperature.

3.2. Optically induced changes in the band structure of $(TaSe_4)_2I$

Figure 3 compares the band dispersion measured by trARPES under different experimental conditions. We focus initially on the effect of the sample temperature. At 27 eV photon energy there is a remarkable difference in intensity between the two linearly dispersing states, the one at larger k_z being barely detectable. At room temperature, in figure 3(a), the IS is still present but, if compared with synchrotron data, a weak spectral weight is visible at E_F due to the lower energy resolution of trARPES. At 80 K in figure 3(b), the intensity near E_F is further reduced, and there is an overall shift towards larger binding energies, in agreement with previous findings [13, 25]. In order to analyze quantitatively the changes induced in the band dispersion by temperature, we extract momentum distribution curves (MDCs) at different binding energies, and fit each curve with a Lorentzian peak and a second order polynomial background. Figures 3(c) and (d)

Figure 3. Optically induced changes in the band structure of $(TaSe_4)_2I$. (a) and (b) Band dispersions measured by trARPES at 27 eV at 300 K (a) and at 80 K (b). (c) and (d) Intensity and position extracted from the analysis of the momentum distribution curves (MDCs) from the 300 K (yellow line) and 80 K (blue line) data. A shaded yellow area highlights the intensity suppression (IS) region. (e) and (f) Snapshots of the band dispersion measured at 80 K, 100 fs after the arrival of the optical excitation with fluence equal to 0 (e) and $0.55\,mJ\,cm^{-2}$ (f). (g) MDCs measured at E_F, at 0.15 eV and at 0.25 eV above E_F, for the two fluences. Electrons are transiently excited in the IS region and in CB above E_F. (h) Fluence dependence of the photoemission intensity measured in $(0.2\,Å^{-1}, 0.12\,eV)$ windows centered along the band dispersion. (i) Difference between the datasets of panels (f) and (e); the color scale encodes the increase (red) and depletion (blue) of the photoemission intensity. (j) and (k) Intensity and position of the bands extracted from the MDC analysis carried out for the datasets at fluence 0 and $0.55\,mJ\,cm^{-2}$. (l) Fluence dependence of the band shift, averaged in the energy region between −0.7 and −0.3 eV, from the datasets at 80 K and 100 fs (upper), at 80 K and −1000 fs (central) and at 300 K and 100 fs (lower).

show the evolution of the intensity and, respectively, the position of the Lorentzian peak. In the fit procedure, the uncertainty in the determination of the peak position is smaller than $0.002\,Å^{-1}$, smaller than the observed shift. Yellow and blue line correspond to the result of the analysis for the data acquired at room temperature and 80 K, respectively. We observe a reduction of spectral weight in the IS region highlighted by the shaded yellow area. In the following we focus on the band dispersion outside the IS region, indicated in figure 3(d) by solid lines.

In a previous ARPES study the temperature dependence of the band gap was extracted from the energy shift of the band leading edge near E_F [25]. Our data show that changes in the dispersion also occur far from E_F, namely a shift of ∼45 meV averaged in the energy region between −0.7 and −0.3 eV. According to theory, this overall shift cannot be ascribed to the structural distortion accompanying the CDW formation. We attribute it instead to the change in electronic screening that follows the opening of the CDW band gap. Therefore, our results establish a connection between changes near E_F and at larger binding energies, which we explore in the following upon an intense optical excitation.

Figures 3(e) and (f) compare snapshots of the band structure 100 fs after optical excitation, at zero (e) and at the largest fluence of $0.55\,mJ\,cm^{-2}$ (f). Following the excitation, electrons populate the linearly dispersing state around E_F, in the IS region. The transient electronic population is more visible in the MDCs of figure 3(g), extracted at E_F, at 0.15 eV and at 0.25 eV above E_F, for the two excitations. Figure 3(i) shows the effect of the optical perturbation as a difference between the two datasets for 0 and $0.55\,mJ\,cm^{-2}$ fluence,
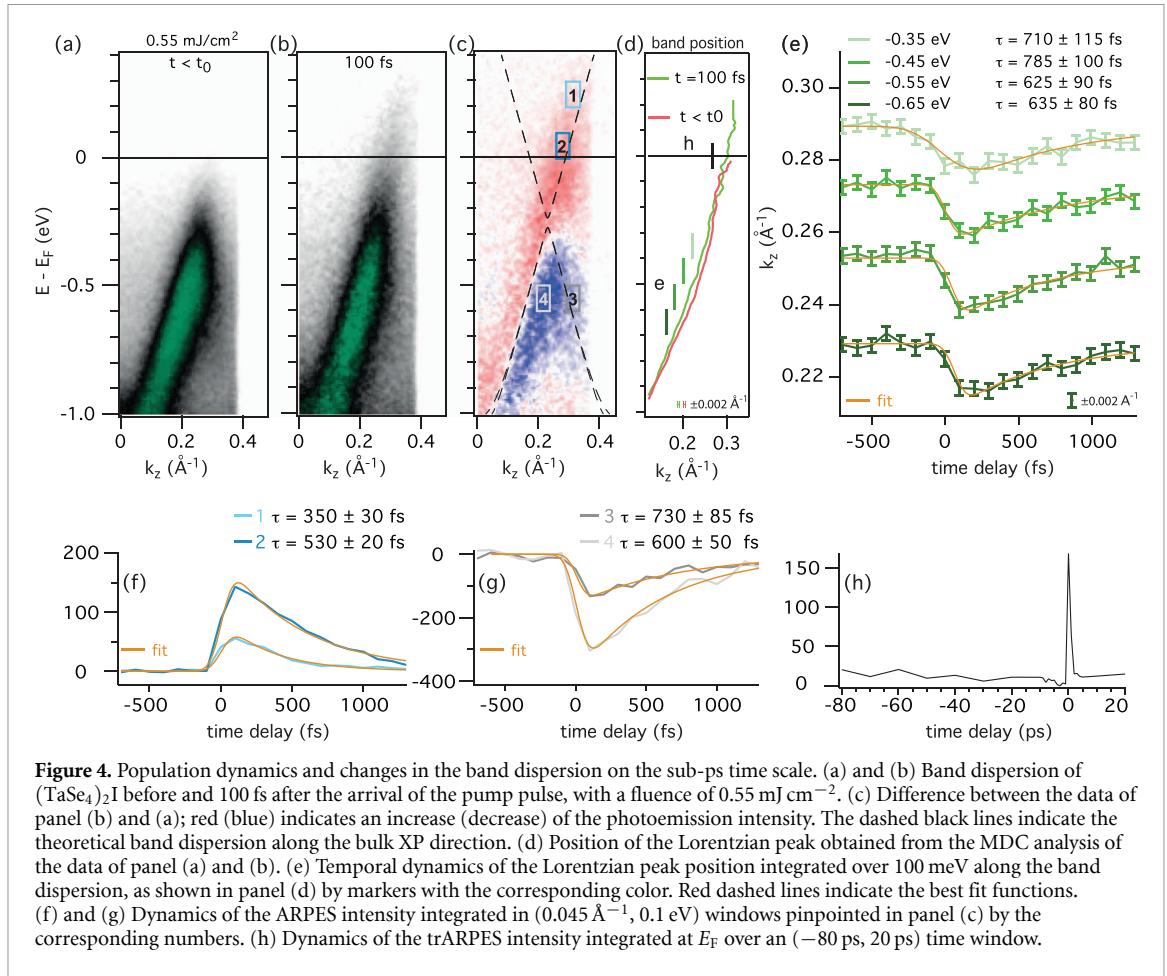
with red (blue) indicating larger (smaller) intensity. In figure 3(h) we monitor the change in electronic populations as a function of the fluence, by integrating the photoemission intensity over $(0.2\,\text{Å}^{-1}, 0.12\,\text{eV})$ windows centered along the band dispersion. We find that both the increase (upper panel) and the depletion (lower panel) of population scale linearly with fluence. In figure 3(i) we observe, for $k_z < \pi/c$, a blue/red signal all along the dispersion of the occupied VB, a common signature of a band-shift, observed in other materials [45–47]. For $k_z > \pi/c$ we observe electrons and holes optically excited in the CB (red) and in the VB (blue). In order to disentangle quantitatively the band-shift from the change in charge population we use again an MDCs analysis. Figures 3(j) and (k) show the change in the intensity and, respectively, the position of the Lorentzian peak. As previously, the uncertainty in the determination of the peak position is smaller than $0.002\,\text{Å}^{-1}$, smaller than the observed shift. The intensity is reduced in the VB, while it increases in the IS region and in the CB above E_F. The band moves towards smaller binding energies by ∼80 meV, as averaged in the energy region between -0.7 and -0.3 eV. We interpret this band-shift as a result of the change in the electronic screening that follows the filling of the CDW band gap. Figure 3(l) shows the dependence of this effect on the fluence at $T = 80\,\text{K}$ (upper panel) and $T = 300\,\text{K}$ (lower panel), respectively.

In general, the energy absorbed by the electrons is expected to be transferred to the lattice by electron-phonon coupling. Phonon anharmonicity and heat transport out of the probed volume are responsible for the recovery of the equilibrium conditions between two subsequent pump pulses. This is however not the case in $(\text{TaSe}_4)_2\text{I}$, and we still observe optically induced changes after 166 μs, corresponding to the temporal separation between two pump pulses. In stroboscopic experiments, the dynamics is accessed by varying the arrival between pump and probe within the same nth laser train pulse. The signal at *negative* delay times bears information on the excitation induced by the $(n-1)$th pump pulse, i.e. on the dynamics at the μs time scale. The central panel of figure 3(l) shows that a band-shift persists at this long time scale, with a smaller but non negligible magnitude of tens of meV at the highest fluence. This is a clear signature of an increase of the lattice temperature. Such temperature build-up reflects the poor thermal conductivity of the compound [48], which cannot dissipate the energy introduced by the optical excitation, compared to conventional semiconductors [49]. The formation in $(\text{TaSe}_4)_2\text{I}$ of a state thermalized at high-temperature was already reported in an ultrafast reflectivity study [50], where the observation of an offset linearly scaling with the fluence was interpreted as a bolometric response of the crystal persisting at the μs time scale. Our trARPES data clarify that this effect is accompanied by an increase of spectral weight at E_F.

3.3. Ultrafast dynamics of the transient changes in the band dispersion of $(\text{TaSe}_4)_2\text{I}$

Here we focus on the ultrashort dynamics of the band-shift, with the goal of separating the fast electronic contribution from the slow component associated to the increase in lattice temperature. Figures 4(a) and (b) compare the band dispersion of $(\text{TaSe}_4)_2\text{I}$ before (-1000 fs) and after (100 fs) the arrival of the pump pulse (t_0) for a fluence of $0.55\,\text{mJ\,cm}^{-2}$. The effect of the excitation is better appreciated from the difference between the two datasets, shown in figure 4(c), where red and blue colors indicate the increase and decrease in intensity, respectively. Dashed black lines trace the theoretical band dispersion along the XP direction. A small stretching (15%) and a shift of the chemical potential (0.3 eV) are applied to improve the agreement with the experiment. The results resemble qualitatively figure 3(i), with the important difference that changes here are over and above the trivial temperature build-up. From the MDC analysis we extract the dynamical change in the position of the Lorentzian peak, shown in figure 4(d). It corresponds to a band shift of ∼40 meV averaged in the energy region between -0.7 and -0.3 eV. The fast component of the band gap renormalization dynamics is illustrated in figure 4(e), which shows the lateral band shift along the band dispersion, averaged over 100 meV windows, at wave vectors indicated by markers of the corresponding colors in figure 4(d). The onset of the band shift coincides with the arrival of the pump pulse within our temporal resolution, and the relaxation is well reproduced by a single exponential decay with characteristic constants in the range 600–800 fs.

Figures 4(f) and (g) show the temporal evolution of the photoemission intensity, integrated in $(0.045\,\text{Å}^{-1}, 0.1\,\text{eV})$ windows indicated in panel (c) by the corresponding numbers. The traces are fitted with a single decaying exponential convoluted with a Gaussian that accounts for the finite temporal resolution, and the best fits are shown in red. Regions 1 and 2 are illustrative of the population dynamics in the CB, and we find that electrons relax with characteristic times in the range 350–530 fs, faster at higher energy above E_F. Regions 3 and 4 show that the photoexcited holes exhibit similar relaxation constants, in the range 600–730 fs. Finally, we investigate the dynamics over a larger temporal window, spanning from -80 ps to 20 ps. Figure 4(h) displays the temporal evolution of the intensity, integrated in a $(0.045\,\text{Å}^{-1}, 0.1\,\text{eV})$ window at E_F, as indicated in panel (d). Besides the sub-ps dynamics around t_0, we do not observe dynamics on longer time scales, possibly due to the relatively short temporal window (80 ps) compared to the μs time scale between pump pulses. The absence of a dynamics for $t < t_0$ rules out the possible influence of

Figure 4. Population dynamics and changes in the band dispersion on the sub-ps time scale. (a) and (b) Band dispersion of $(TaSe_4)_2I$ before and 100 fs after the arrival of the pump pulse, with a fluence of 0.55 mJ cm^{-2}. (c) Difference between the data of panel (b) and (a); red (blue) indicates an increase (decrease) of the photoemission intensity. The dashed black lines indicate the theoretical band dispersion along the bulk XP direction. (d) Position of the Lorentzian peak obtained from the MDC analysis of the data of panel (a) and (b). (e) Temporal dynamics of the Lorentzian peak position integrated over 100 meV along the band dispersion, as shown in panel (d) by markers with the corresponding color. Red dashed lines indicate the best fit functions. (f) and (g) Dynamics of the ARPES intensity integrated in (0.045 Å^{-1}, 0.1 eV) windows pinpointed in panel (c) by the corresponding numbers. (h) Dynamics of the trARPES intensity integrated at E_F over an $(-80$ ps, 20 ps) time window.

pump-induced space-charge [51] and surface photovoltage effects [52, 53], which are both known to cause shifts in the band structure with a characteristic dynamics of tens of ps at negative delay times.

We observe that the time scale of the electron dynamics in the CB is similar to the ultrafast dynamics of the band-shift, suggesting that the two phenomena are related. This supports our interpretation of the band-shift in terms of a change in the electronic screening, which can arise both from a change in the CDW band gap and from the presence of high-energy electrons transiently populating the CB, as recently found in other systems with linearly dispersing Dirac particles [54, 55]. On a longer time scale the band-shift is dominated by the change in screening due to modification of the temperature-dependent CDW band gap, which follows the heat accumulation in the lattice due to the poor thermal conductivity. Finally, we notice that the two effects, the ultrafast and the persistent components of the band-shift, are comparable in magnitude. By directly assessing the transient change in the band structure, our results confirm the conclusion drawn by an all-optical time-resolved reflectivity study [50]. According to that investigation, an excitation fluence of 0.4 mJ cm^{-2} corresponds to an increase of energy per unit cell of $\sim$100 meV, comparable to the electronic part of the condensation energy calculated in the mean-field limit, and it is therefore sufficient to melt the CDW state [50]. This shows that an optical excitation provides a way to control the band gap of $(TaSe_4)_2I$ and the spectral weight at the Fermi level. In our opinion our results provide a possible explanation for the good photo-response behavior of the material. A recent work has shown that photocurrent is generated by photo-bolometric effect upon illumination with visible (683 nm) and infrared light (980 nm) with fluences comparable to the ones used in our study [33]. The performances of $(TaSe_4)_2I$ are found to be comparable or even better than other materials used as IR photodetectors. Weyl semimetals thus represent promising candidates for several applications in optoelectronics operating at different time scales, ranging from the μs dynamics of $(TaSe_4)_2I$ to the sub-100 fs modulation of the optical properties of NbP thin films [56].

4. Conclusion

We have used trARPES to perturb the CDW state that gaps the Weyl points in $(TaSe_4)_2I$. Upon optical excitation, we see electrons filling the gap region and populating the CB above E_F, and an overall energy shift

of the occupied VB. We report an ultrafast dynamics that relaxes at the sub-ps time scale, reflecting the change in screening due to the filling of the CDW band gap and to the transient population of the CB. At longer time scales, the energy left by the pump in the electronic bath is transferred to the lattice where it accumulates, building up an increase in lattice temperature. This optically induced change in temperature causes a band shift that persists at the μs time scale. It indicates that the lattice of $(TaSe_4)_2I$ cannot efficiently remove energy from the probed volume. This effect could also influence the electronic transport measurements in conditions of large Joule power dissipation, as recently pointed out by Sinchenko *et al* [14]. Understanding the origin of this effect is therefore important to improve transport experiments that probe the axionic insulators. It would require further investigations of the phonon anharmonicity and heat diffusion in the material, beyond the scope of this work.

Our results show that optical excitation provides a viable tool to modify the band dispersion of $(TaSe_4)_2I$ at the ultrafast time scale and with changes that persist for several hundreds of μs. Therefore, light can be used to melt the CDW order in $(TaSe_4)_2I$ and this could be combined with ultrafast transport measurements to access the topological phase transition. Finally, our observation of an optically-induced increase in spectral weight at E_F shines light on the microscopic mechanisms responsible for the high performances of $(TaSe_4)_2I$ as a near-infrared photodetector [33].

Data availability statement

The data that support the findings of this study are available upon reasonable request from the authors.

Acknowledgments

ORCID iDs

A Crepaldi ⦿ https://orcid.org/0000-0001-9971-1731
M Puppin ⦿ https://orcid.org/0000-0002-1328-7165
L Moreschini ⦿ https://orcid.org/0000-0001-8226-084X
O V Yazyev ⦿ https://orcid.org/0000-0001-7281-3199

References

[1] Wan X, Turner A M, Vishwanath A and Savrasov S Y 2011 *Phys. Rev.* B **83** 205101
[2] Xu S Y *et al* 2015 *Science* **349** 613–7
[3] Armitage N P, Mele E J and Vishwanath A 2018 *Rev. Mod. Phys.* **90** 015001
[4] Burkov A 2018 *Annu. Rev. Condens. Matter Phys.* **9** 359–78
[5] Burkov A 2015 *J. Phys.: Condens. Matter* **27** 113201
[6] Wilczek F 1987 *Phys. Rev. Lett.* **58** 1799–802
[7] Peccei R D and Quinn H R 1977 *Phys. Rev. Lett.* **38** 1440–3
[8] Preskill J, Wise M B and Wilczek F 1983 *Phys. Lett.* B **120** 127–32
[9] Qi X L, Hughes T L and Zhang S C 2008 *Phys. Rev.* B **78** 195424
[10] Nenno D M, Garcia C A C, Gooth J, Felser C and Narang P 2020 *Nat. Rev. Phys.* **2** 682–96
[11] Wang Z and Zhang S C 2013 *Phys. Rev.* B **87** 161107
[12] Gooth J *et al* 2019 *Nature* **575** 315–9
[13] Shi W *et al* 2021 *Nat. Phys.* **17** 381–7
[14] Sinchenko A A, Ballou R, Lorenzo J E, Grenet T and Monceau P 2022 *Appl. Phys. Lett.* **120** 063102
[15] Monceau P 2012 *Adv. Phys.* **61** 325–581
[16] Fujishita H, Sato M and Hoshino S 1984 *Solid State Commun.* **49** 313–6
[17] Wang Z Z, Saint-Lager M C, Monceau P, Renard M, Gressier M, Meerschaut A, Guemas L and Rouxel J 1983 *Solid State Commun.* **46** 325–8
[18] Favre-Nicolin V, Bos S, Lorenzo J E, Hodeau J L, Berar J F, Monceau P, Currat R, Levy F and Berger H 2001 *Phys. Rev. Lett.* **87** 015502
[19] Lorenzo J E, Currat R, Monceau P, Hennion B, Berger H and Levy F 1998 *J. Phys.: Condens. Matter* **10** 5039
[20] Gressier P, Whangbo M H, Meerschaut A and Rouxel J 1984 *Inorg. Chem.* **23** 1221–8
[21] Grioni M, Pons S and Frantzeskakis E 2008 *J. Phys.: Condens. Matter* **21** 023201
[22] Voit J, Perfetti L, Zwick F, Berger H, Margaritondo G, Grüner G, Hochst H and Grioni M 2000 *Science* **290** 501–3

[23] Zhang Y, Lin L F, Moreo A, Dong S and Dagotto E 2020 *Phys. Rev.* B **101** 174106
[24] Tournier-Colletta C *et al* 2013 *Phys. Rev. Lett.* **110** 236401
[25] Perfetti L, Berger H, Reginelli A, Degiorgi L, Höchst H, Voit J, Margaritondo G and Grioni M 2001 *Phys. Rev. Lett.* **87** 216404
[26] Huang Z, Yi H, Min L, Mao Z, Chang C Z and Wu W 2021 *Phys. Rev.* B **104** 205138
[27] Lee P A, Rice T M and Anderson P W 1973 *Phys. Rev. Lett.* **31** 462–5
[28] Schwartz A *et al* 1995 *Phys. Rev.* B **52** 5643–52
[29] Schmitt F *et al* 2008 *Science* **321** 1649–52
[30] Petersen J C *et al* 2011 *Phys. Rev. Lett.* **107** 177402
[31] Hellmann S *et al* 2012 *Nat. Commun.* **3** 1069
[32] Hedayat H *et al* 2019 *Phys. Rev. Res.* **1** 023029
[33] Cheng J *et al* 2021 *Appl. Phys. Lett.* **119** 201909
[34] Gressier P, Guemas L and Meerschaut A 1982 *Acta Crystallogr.* B **38** 2877–9
[35] Crepaldi A *et al* 2017 *Chimia* **71** 273–7
[36] Giannozzi P *et al* 2009 *J. Phys.: Condens. Matter* **21** 395502
[37] Giannozzi P *et al* 2017 *J. Phys.: Condens. Matter* **29** 465901
[38] Perdew J P, Burke K and Ernzerhof M 1996 *Phys. Rev. Lett.* **77** 3865
[39] Corso A D 2014 *Comput. Mater. Sci.* **95** 337–50
[40] Chang G *et al* 2018 *Nat. Mater.* **17** 978–85
[41] Gatti G *et al* 2020 *Phys. Rev. Lett.* **125** 216402
[42] Yi H *et al* 2021 *Phys. Rev. Res.* **3** 013271
[43] Bedoya-Pinto A, Pandeya A K, Liu D, Deniz H, Chang K, Tan H, Jena J, Kostanovskiy I and Parkin S S P 2020 *ACS Nano* **14** 4405–13
[44] Bedoya-Pinto A, Liu D, Tan H, Pandeya A K, Chang K, Zhang J and Parkin S S P 2021 *Adv. Mater.* **33** 2008634
[45] Manzoni G *et al* 2015 *Phys. Rev. Lett.* **115** 207402
[46] Ulstrup S *et al* 2016 *ACS Nano* **10** 6315–22
[47] Roth S *et al* 2019 *2D Mater.* **6** 031001
[48] Kwok R S and Brown S E 1989 *Phys. Rev. Lett.* **63** 895–8
[49] Holland M G 1964 *Phys. Rev.* **134** A471–80
[50] Schaefer H, Koerber M, Tomeljak A, Biljaković K, Berger H and Demsar J 2013 *Eur. Phys. J. Spec. Top.* **222** 1005–16
[51] Oloff L P, Hanff K, Stange A, Rohde G, Diekmann F, Bauer M and Rossnagel K 2016 *J. Appl. Phys.* **119** 225106
[52] Yang S-L, Sobota J A, Kirchmann P S and Shen Z-X 2014 *Appl. Phys.* A **116** 85–90
[53] Ulstrup S *et al* 2015 *J. Electron Spectrosc. Relat. Phenom.* **200** 340–6
[54] Gatti G *et al* 2020 *Phys. Rev. Lett.* **125** 076401
[55] Nilforoushan N *et al* 2020 *Phys. Rev. Res.* **2** 043397
[56] Tilmann B, Pandeya A K, Grinblat G, Menezes L D S, Li Y, Shekhar C, Felser C, Parkin S S P, Bedoya-Pinto A and Maier S A 2022 *Adv. Mater.* **34** 2106733